

Tmprss3 loss of function impairs cochlear inner hair cell Kcnma1 channel membrane expression

Laurence Molina^{1,†}, Lydie Fasquelle^{2,3,†}, Régis Nouvian^{2,3}, Nicolas Salvetat¹, Hamish S. Scott^{4,5}, Michel Guipponi⁶, Franck Molina¹, Jean-Luc Puel^{2,3} and Benjamin Delprat^{2,3,*}

¹SysDiag UMR 3145 CNRS/Bio-Rad, Cap Delta/Parc Euromédecine, 1682 rue de la Valsière, CS 61003, Cedex 4, Montpellier 34184, France, ²Inserm U 1051, Institut des Neurosciences de Montpellier, Hôpital Saint Eloi, Montpellier 34091, France, ³Université de Montpellier, Montpellier 34091, France, ⁴Department of Molecular Pathology, The Centre for Cancer Biology, SA Pathology and Box 14 Rundle Mall Post Office, Adelaide, South Australia 5000, Australia, ⁵The Schools of Medicine and Molecular and Biomedical Science, The University of Adelaide, Adelaide, South Australia 5005, Australia and ⁶Department of Genetic Medicine and Development, University of Geneva Medical School and University Hospitals of Geneva, 4 Geneva 1211, Switzerland

Received October 25, 2012; Revised and Accepted December 12, 2012

Before acquiring their mature state, cochlear hair cells undergo a series of changes in expression of ion channels. How this complex mechanism is achieved is not fully understood. *Tmprss3*, a type II serine protease expressed in hair cells, is required for their proper functioning at the onset of hearing. To unravel the role of *Tmprss3* in the acquisition of mature K^+ currents, we compared their function by patch-clamp technique in wild-type *Tmprss3*^{WT} and *Tmprss3*^{Y260X}-mutant mice. Interestingly, only outward K^+ currents were altered in *Tmprss3*^{Y260X}-mutant mice. To determine by which mechanism this occurred, we compared the protein network of *Tmprss3*^{WT} and *Tmprss3*^{Y260X}-mutant mice using proteomic analysis. This led to the identification of a pathway related to potassium *Kcnma1* channels. This pathway was validated by immunohistochemistry, focusing on the most downregulated protein that was identified as a cochlear *Kcnma1*-associated protein, APOA1. Finally, we show that, in contrast to *Tmprss3*^{WT}, *Kcnma1* channels were absent at the neck of inner hair cells (IHCs) in *Tmprss3*^{Y260X}-mutant mice. In conclusion, our data suggest that lack of *Tmprss3* leads to a decrease in *Kcnma1* potassium channels expression in (IHCs).

INTRODUCTION

The perception of sound relies on the proper functioning of the cochlea, the peripheral auditory organ. In mammalian cochlea, inner hair cells (IHCs) translate sound stimulation into graded receptor potentials. At the onset of hearing (P10–P12 in mice), IHCs undergo massive changes in their electrical properties (1,2), and notably, the maturation of hair cells correlates with the expression of large outward-rectifying potassium currents, $I_{K,f}$, carried by *Kcnma1* channels (3). The fast activation kinetics of these channels shape the time course and amplitude of the hair cell receptor potential (4), indicating that *Kcnma1* channels in hair cells are critical for high-fidelity sound encoding. At the same time $I_{K,n}$ current is expressed to set the resting

potential of IHCs (5,6). This current is generated by KCNQ4 whose mutations are responsible for DFNA2 human deafness (7). Finally, a classical delayed-rectifier K^+ current, name $I_{K,s}$ shows slow activation kinetics and represents the slow component of the K^+ outward current (3).

Mutations in the *TMPRSS3* gene were shown to cause human autosomal recessive non-syndromic deafness (DFNB8/10) (8), characterized by bilateral, severe to profound hearing loss. To address the role of the protein in the cochlear physiology, we generated an ethylnitrosurea (ENU) C3HeB/FeJ-mutant mouse (9). A T to A substitution in exon 7, resulting in a nonsense mutation at tyrosine 260 was identified (*Tmprss3*^{Y260X}) that would result in the production of a 194 amino acid truncated protein, deleted of most of its protease domain (9).

*To whom correspondence should be addressed at: Inserm U1051, 80 rue Augustin Fliche, Montpellier 34091, France. Tel: +33 499636061; Fax: +33 499636020; Email: benjamin.delprat@inserm.fr

†These authors contributed equally to this work.

The analysis of the *Tmprss3*^{Y260X}-mutant mice revealed that *Tmprss3* is essential for mouse cochlear hair cell survival at the onset of hearing and that *Tmprss3* mutations induce deafness in mice (9) and in humans. Indeed, in the *Tmprss3*^{Y260X}-mutant mice, hair cells degenerate drastically in 2 days (between P12 and P14). Thus, *Tmprss3* is expressed in cochlear hair cells in the developing cochlea and at the onset of hearing, suggesting that *Tmprss3* may be a hair cell-autonomous survival factor (9). We also identified a novel, longer *Tmprss3* isoform with a 22 amino acid extension at the N-terminal, namely *Tmprss3f*. This isoform is expressed predominantly in the cochlea in contrast to the shorter isoform that is expressed broadly, suggesting a specific role of *Tmprss3f* in hair cell functioning and/or survival (9). Finally, the only known substrate of TMPRSS3 that was observed in *Xenopus* oocytes (10) is the epithelial amiloride-sensitive sodium channel (ENaC).

Because IHC maturation is dependent on a change in ionic conductance expression, and given that *Tmprss3* is known to activate ENaC channels in *Xenopus* oocytes, we would like to determine whether *Tmprss3* was able to modulate the function of channels or channel regulatory proteins in IHCs. Using an integrated approach combining the patch-clamp technique, two-dimensional (2D) gels followed by mass spectrometry analysis, bioinformatic functional studies and immunohistochemistry, we showed, for the first time, that *Tmprss3* loss of function leads to a decrease in the IHCs' Kcnma1 channel plasma membrane expression. These alterations were associated with the downregulation of ApoA1 in IHCs, which is a protein identified as a Kcnma1 channel interacting partner expressed in IHCs (11).

Our data highlight a novel link between Kcnma1 channels and a serine protease. This unique finding suggests that this original relationship seems highly important for the normal physiology of IHCs and it should be significant for other essential body functions, where Kcnma1 channels play a key role, such as neurotransmission (12), blood flow (13), urine flow (14) and immunity (15).

RESULTS

Lack of fast K⁺ conductance in *Tmprss3*^{Y260X} mouse IHCs

Because ENaC, the only known substrate of *Tmprss3*, is not expressed in cochlear hair cells (16–18), whole-cell patch-clamp recordings were used to probe the K⁺ current in P13-old apical IHCs before degenerative changes occurred in this region of the cochlea (9). When depolarized, IHCs from *Tmprss3*^{WT} showed an outward K⁺ current with a fast activating outward component, reminiscent of Kcnma1 currents (3,4,19) and a more slowly activating component (Fig. 1A). IHCs from *Tmprss3*^{Y260X} showed a drastic reduction in the amplitude of the outward currents when measured 1 ms after the start of the depolarizing pulses (mostly recruiting Kcnma1 channels activation; 4.6 ± 0.4 nA at 30 and 2.27 ± 0.15 nA at 37 mV in *Tmprss3*^{WT} and *Tmprss3*^{Y260X}, respectively, Fig. 1B–D). In contrast, the magnitudes of the currents at the end of the depolarizing pulses were comparable between the genotypes (Fig. 1D). The difference of K⁺ outward current observed between the *Tmprss3*^{WT} and *Tmprss3*^{Y260X} could be explained by a delayed

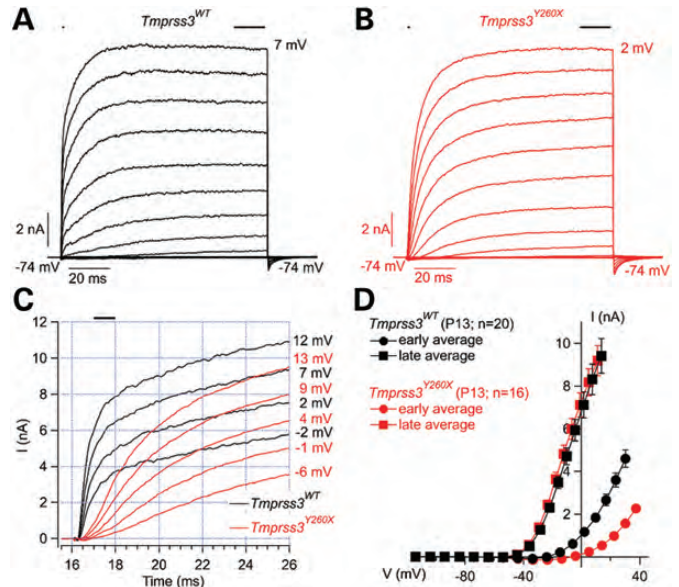


Figure 1. IHCs K⁺ current analysis of *Tmprss3*^{WT} and *Tmprss3*^{Y260X} mice. (A and B) Representative outward currents recorded from P13 *Tmprss3*^{WT} (A, black) and *Tmprss3*^{Y260X} (B, red) IHCs. K⁺ currents were evoked by 100 ms long-step depolarizations from -114 mV to the indicated potentials (voltage increments of 10 mV, holding potential of -74 mV). (C) First 10 ms of these outward currents recordings on an expanded time scale. *Tmprss3*^{WT} (black) and *Tmprss3*^{Y260X} (red). (D) Mean I/V relationships for *Tmprss3*^{WT} (black) and *Tmprss3*^{Y260X} (red) IHCs obtained by averaging currents 1 ms after the start of the depolarizing pulses over 1 ms (filled circles, early average) and over the last 15 ms of depolarization steps (filled squares, late average). The mean series resistance of *Tmprss3*^{WT} (black) and *Tmprss3*^{Y260X} (red) IHCs was 3.4 ± 0.1 M Ω and 3.8 ± 0.1 M Ω , respectively, after Rs compensation, and data were corrected offline for the remaining voltage error and liquid junction potential (-4 mV). Resting membrane capacitance of *Tmprss3*^{WT} (black) and *Tmprss3*^{Y260X} (red) was 9.4 ± 0.1 pF and 8.1 ± 0.2 pF, respectively ($n = 20$ for *Tmprss3*^{WT}, $n = 16$ for *Tmprss3*^{Y260X}). The difference is statistically significant (two sample *t*-test, $P < 0.05$).

maturation. However, exocytosis triggered by Ca²⁺ currents was similar between *Tmprss3*^{WT} and *Tmprss3*^{Y260X} in P9–P11-old IHCs (Data not shown), suggesting normal hair cell development (20). Current-clamp recordings ($I_{inj} = 0$ pA) indicated no difference in the resting membrane potential of the IHCs between both genotypes (-69.4 ± 1.3 mV and -67.9 ± 2.1 mV for *Tmprss3*^{WT} and *Tmprss3*^{Y260X} IHCs, respectively).

Differential proteomics

To identify proteins that could regulate the expression of IHC K⁺ channels and that are linked to *Tmprss3*, P10 mouse cochlea extracts from *Tmprss3*^{WT} and *Tmprss3*^{Y260X} were analyzed by a proteomic approach using 2D-gel electrophoresis (2D-GE). We chose P10 because it represents a good compromise between the presumed absence of the apoptosis-related proteins that may be present in cochlear extracts at P12 due to the beginning of hair cell degeneration, and the presence of mature K⁺ currents that begin to appear at P10. After image analysis, more than 2000 spots were detected from cochlea extracts with a wide range of molecular weights (15–150 kDa) and isoelectric points (3–10 pI). To compare the *Tmprss3*^{WT} and *Tmprss3*^{Y260X} proteomes, it was

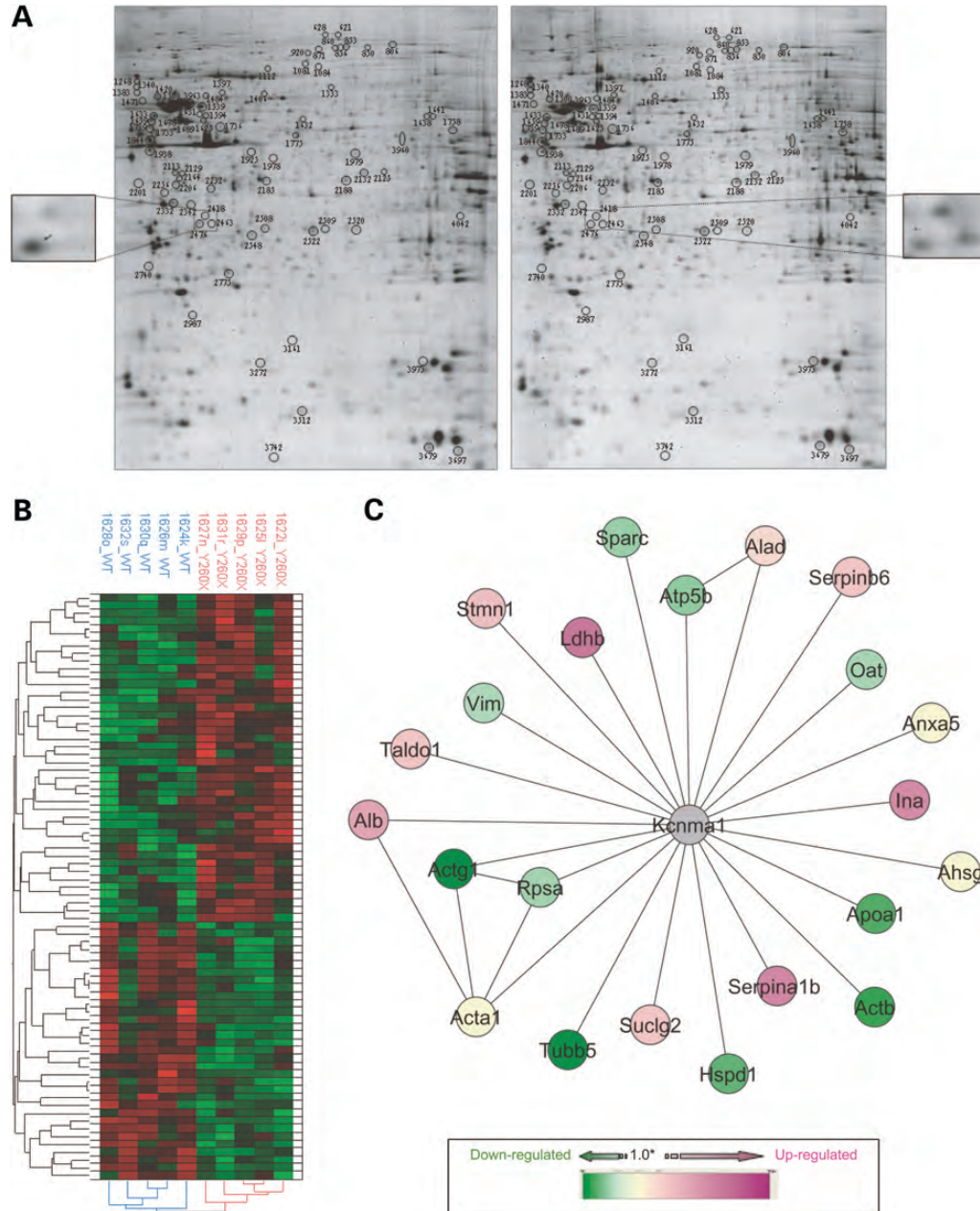


Figure 2. Proteomic analysis and altered pathway in *Tmprss3*^{Y260X}-mutant mice. **(A)** 2D-GE of proteins extracted from *Tmprss3*^{WT} cochlea (left gel) and *Tmprss3*^{Y260X} cochlea (right gel). Seventy-seven protein spots were differentially expressed, and protein spots were up or downregulated (example of spot regulation in the side inset). The proteins of interest identified by LC-MS/MS are shown on the gels by a circle. **(B)** Heat map and HAC of the 77 protein spots present in all cochlea 2D-GE. The intensity levels of the protein spots *p* were visualized by a heat map and HAC analysis using the JMP v8 software. Each column represents the data from one 2D-GE experiment. Rows represent individual spots. Raw data were mean centered, and the graduated scale color codes from green (low level of intensity) to red (high level of intensity). **(C)** Network of identified proteins connected to *Kcnma1*. Nodes and edges are represented by gray circles and black lines, respectively. Identified proteins differentially expressed between *Tmprss3*^{WT} and *Tmprss3*^{Y260X} were highlighted using a graduated scale from green (downregulated) to pink (upregulated) according to their fold ratio. Proteins that were both up and downregulated in different protein spots were represented by a ratio of 1 (yellow). Some edges may represent a set of different PPIs found in the database. View of the merged network imported from Cytoscape using the IntAct and BioGRID databases.

important to firstly assess the consistency of our dataset after 2D-GE separation. To this end, we used a dispersion tree approach (20), and the 10 2D-GE experiments were dispersed homogeneously on the 10 branches of the tree, which formed a circle (Supplementary Material, Fig. S1A). The homogeneity of the data was also confirmed by three other

statistical methods: the Mahalanobis distance, principal component analysis and Pearson correlation (Supplementary Material, Fig. S1B–D).

In the comparative analysis of all protein spots between *Tmprss3*^{WT} and *Tmprss3*^{Y260X}, 77 distinct protein spots were differentially expressed (Fig. 2A). To visualize these protein

spots further, we clustered the high-confidence dataset of 77 protein spots. The dataset was then subjected to hierarchical clustering analysis generating the heat map and the dendrogram shown in Figure 2B. Two main clusters of protein spots were clearly detected and differentially regulated. These two clusters corresponded to upregulated proteins in the presence of *Tmprss3*^{Y260X} (high intensity shown in red) and to downregulated proteins (low intensity shown in green). Thirty-three protein spots were downregulated and 44 were upregulated in *Tmprss3*^{Y260X} mice. All the differentially regulated protein spots were identified by liquid chromatography coupled to tandem mass spectrometry (LC-MS/MS) analysis, and the results are summarized in the Supplementary Material, Table S1. One hundred and nineteen independent proteins were identified (after excluding redundant proteins) because of the presence of several spots containing more than one type of identification. Indeed, some proteins were present in full size form and/or in fragment form, such as vimentin and tubulin beta-5, and others were present in different pI forms such as transaldolase 1 and sparc. Moreover, proteins that were upregulated in a spot and downregulated in another one were represented by a fold ratio of one. Less than 1% of proteins identified in our screen are related to apoptosis, suggesting that the altered expression of the proteins is due to a lack of function of *Tmprss3*, rather than a degenerative process initiated by the IHCs.

Perturbed network identification

To evaluate the potential functional relationships between the set of identified proteins, we carried out a gene ontology (GO) enrichment analysis. We then used the Ontologizer software to perform a statistical analysis of the mapping of the 119 identified proteins over the functional GO terms (Supplementary Material, Table S2). Subsequently, we built a wider network by looking at connected proteins (first-degree neighbors) with our set of 119 identified proteins using the IntAct and BioGRID merge network. The average degree of connectivity of the new network (Supplementary Material, Fig. S2) supported the potential functional relationships between differentially expressed proteins found in the Y260X-mutated mouse versus the wild type (WT). This new network (Supplementary Material, Fig. S2) contained **191** proteins connected with **68** identified proteins. In this network, the identified proteins were connected to each other at the most with second-degree neighbors (via a single intermediary). Out of **191** proteins, **160** were present in a main connected subnetwork corresponding to **52** identified proteins, with 23 upregulated, 23 downregulated and 6 up and downregulated. The other subnetworks, containing at least one identified protein, were composed of a maximum of two to five interactions, or of isolated proteins. In addition, **51** identified proteins did not have any currently documented interaction partners referenced in the IntAct and BioGRID databases. From the main subnetworks (**160** proteins), only 4 highly connected 'hub' proteins were identified. These 'hubs' were Ywhab, Ywhaz, Dlh4 and *Kcnma1* corresponding to the following proteins: 14-3-3 protein beta/alpha (Ywhab), 14-3-3 protein zeta/delta (Ywhaz), disks large homolog 4 (Dlg4/PSD95) and calcium-activated potassium channel sub-unit alpha-1 (*Kcnma1*) connecting 17, 5, 13 and

22 identified proteins, respectively (Fig. 2C and Supplementary Material, Fig. S2). Interestingly, *Kcnma1* protein connected the largest number of identified proteins from comparative 2D-GE analysis between *Tmprss3*^{WT} and *Tmprss3*^{Y260X}.

APOA1 is downregulated in *Tmprss3*^{Y260X}-mutant mice

Among the proteins identified by mass spectrophotometry, APOA1 was the most known cochlear interacting protein of *Kcnma1*, which was downregulated. To validate the APOA1 regulation by *Tmprss3*, immunohistochemistry was implemented on P13 cochlear explants. Using a polyclonal antibody, APOA1 (red) seemed to be expressed mainly in the IHCs of *Tmprss3*^{WT} mice labeled with a monoclonal parvalbumin antibody (green) (Fig. 3A). This expression pattern is expected as APOA1 has been shown to be expressed in the cytoplasm of mouse IHC (11). In contrast, APOA1 labeling was fainter in the remaining *Tmprss3*^{Y260X} IHCs (Fig. 3B). Indeed, the total intensity of the APOA1 signal inside each IHC is greater in *Tmprss3*^{WT} mice than in *Tmprss3*^{Y260X} mice (Fig. 3C). Because ApoA1 is known to interact with *Kcnma1* channels (11), the downregulation of ApoA1 in *Tmprss3*^{Y260X} mice suggests that *Tmprss3* impairs the *Kcnma1* channel's interactome.

Kcnma1 channels are not clustered in puncta in *Tmprss3*^{Y260X} mouse IHCs

It is well known that *Kcnma1* channel immunoreactivity is clustered in puncta in the neck of mammalian IHCs (19). Therefore, it is possible to determine whether *Kcnma1* channels are correctly expressed in the IHCs of *Tmprss3*^{Y260X}-mutant mouse. To address this question, immunohistochemical staining of the *Kcnma1* channel using a monoclonal anti-*Kcnma1* antibody was used in the developing *Tmprss3*^{WT} and *Tmprss3*^{Y260X} organ of Corti in the same cochlear turn from P12 to P14 (Fig. 4). Indeed, as there were no more hair cells from P15 in *Tmprss3*^{Y260X}-mutant mice, we did not pursue our study further after P14. At P12, the period corresponding to the onset of hearing in mice, some *Tmprss3*^{WT} IHCs expressed *Kcnma1* channels in their neck (Fig. 4A). In contrast, no *Tmprss3*^{Y260X} IHCs expressed *Kcnma1* channels at this stage (Fig. 4B). At P13, more *Tmprss3*^{WT} IHCs expressed *Kcnma1* channels, and the number of puncta increased per hair cell (Fig. 4C). As at P12, no P13 *Tmprss3*^{Y260X} IHCs expressed *Kcnma1* channels (Fig. 4D), but signs of IHCs that had degenerated were observed. Finally, at P14, all *Tmprss3*^{WT} IHCs expressed *Kcnma1* channels, and the number of puncta increased (Fig. 4E). At P14 in *Tmprss3*^{Y260X} IHCs, the majority of IHCs had degenerated, but in the persisting IHCs, no *Kcnma1* channel expression was observed (Fig. 4F). We quantified the number of IHCs expressing *Kcnma1* channels in their neck depending on the cochlear turn and the age of the animals (see Fig. 4G). The number of IHCs expressing *Kcnma1* channels is greater in the basal turn of the cochlea than in the apical one and increased from P12 to P14 as previously observed (19).

DISCUSSION

The lack of expression of *Kcnma1* channels at the plasma membrane may be due to defects of various cellular processes.

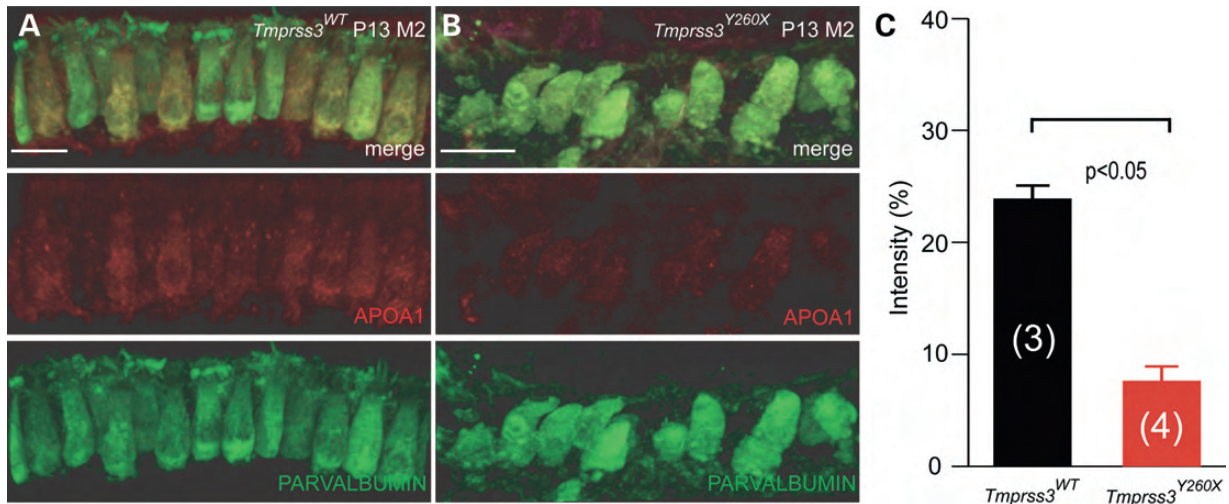


Figure 3. APOA1 is downregulated in IHCs *Tmprss3*^{Y260X}-mutant mice. Cochlear explants were stained with anti-APOA1 antibody in P13 mice. (A) APOA1 (red) is expressed mainly in IHCs, identified by parvalbumin labeling (green) in *Tmprss3*^{WT} cochlea. (B) Less staining could be observed in the remaining IHCs of *Tmprss3*^{Y260X}-mutant mice. (C) Quantification of the intensity of APOA1 labeling in hair cells in *Tmprss3*^{WT} (24%) and *Tmprss3*^{Y260X}-mutant mice (7.6%). The percentage corresponds to the percentage of red color ($n = 3$ for *Tmprss3*^{WT}, $n = 4$ for *Tmprss3*^{Y260X}). The difference is statistically significant (two sample Wilcoxon test, $P < 0.05$).

One hypothesis may be that as the hair cells begin to degenerate, the consequence will be an altered expression of Kcnma1 channels. Our data show that only Kcnma1 channels are lacking—the delayed rectifier K^+ channel is still present as is the calcium channel Cav1.3 (this study). However, specific abolition of Kcnma1 channels when cochlear hair cells are degenerating has never been reported to our knowledge. Moreover, in *Beethoven* mutant mice, hair cells still have residual $I_{K,f}$ current just before their degeneration (21). Hence, it is unlikely that the specific lack of Kcnma1 channels is due to the degeneration of cochlear hair cells. Another hypothesis is that *Tmprss3*^{Y260X} hair cell maturation fails or is delayed as IHCs from *Tmprss3*^{Y260X} are smaller than WT littermate. Indeed, genetic ablation of the calcium channel Cav1.3 sub-unit (19), and its associated β -2 sub-unit (22), ER transmembrane protein Tmc1 (21), molecular motor Myo6 (23), actin-binding protein (24), or thyroid hormone receptor (25) leads to the absence of $I_{K,f}$ current because of a failure or a delay in cochlear hair cell maturation. However, transmission electron microscopy observations of *Tmprss3*^{Y260X} IHCs show normal development until their degeneration [(presence of small numbers of ribbons/IHCs, mature synaptic contacts with only one ribbon/synapse, efferent synaptic contact onto lateral afferent under IHC and direct efferent synaptic contact onto OHC (9)], and normal I_{Ca} current amplitude and normal exocytosis were measured in *Tmprss3*^{Y260X} when compared with *Tmprss3*^{WT} (this study). All these observations suggest involvement of other mechanisms besides maturation failure or delay.

Observing our differentially expressed protein data, we identified proteins associated with Kcnma1 channels that may modulate the membrane expression of channels and transporters. Indeed, 15 out of 119 and 13 out of 119 of the proteins identified in the present screen were identified previously as Kcnma1 channel interacting partners that originated from membrane/cytoskeletal and cytoplasmic fraction, respectively

(26,27). These data suggest that *Tmprss3* is a part of Kcnma1 channel pathway and that loss of function of *Tmprss3* interferes with proper Kcnma1 channel membrane expression. Interestingly, three proteins identified in our screen induce deafness either in humans (γ actin and serpinb6) or mice (β actin). *ACTG1* (γ actin) was identified as the causative gene of DFNA20/26 human deafness (28) and in the syndromic deafness form of Baraitser-Winter Syndrome 2 (29). All DFNB20/26 patients display progressive, bilateral, sensorineural hearing loss that begins in the high frequencies. As age increases, the degree of hearing loss increases, with threshold shifts seen at all frequencies (28). In contrast, congenital or late-onset progressive hearing loss is a common feature of Baraitser-Winter syndrome 2. *Actg1* is essential for the stereocilia maintenance in mice (30), but not their normal development. However, *Tmprss3*^{Y260X}-mutant mice have normal stereocilia (9). Interestingly, downregulation of *Actg1*, which interacts with Kcnma1, decreases Kcnma1 channel membrane expression in transfected CHO cells (27). As *Actg1* is downregulated in our screen, it is tempting to speculate that *Tmprss3* affects the distribution of *Actg1* that in turn affects the proper expression of Kcnma1 channel at the inner hair cell plasma membrane. *ACTB* (β actin) mutations cause Baraitser-Winter Syndrome 2 (29). *Actb* is also required for stereocilia maintenance, and mutations in mice lead to progressive deafness (30). Like *Actg1*, *Actb* interacts with Kcnma1, and its downregulation in podocytes decreases Kcnma1 surface expression (31). As *Actb* is downregulated in our proteomic screen, this may lead to a decreased expression of Kcnma1 at the inner hair cell surface. Interestingly, *Eps8*, a protein with actin binding, bundling, and barbed-end capping activities is a novel component of the hair bundle that is localized predominantly at the tip of the stereocilia and is essential for its normal elongation and function (24). Surprisingly, IHCs from *Eps8* knockout mice do not develop adult-type ion channels (lack of $I_{K,f}$ conductance linked to

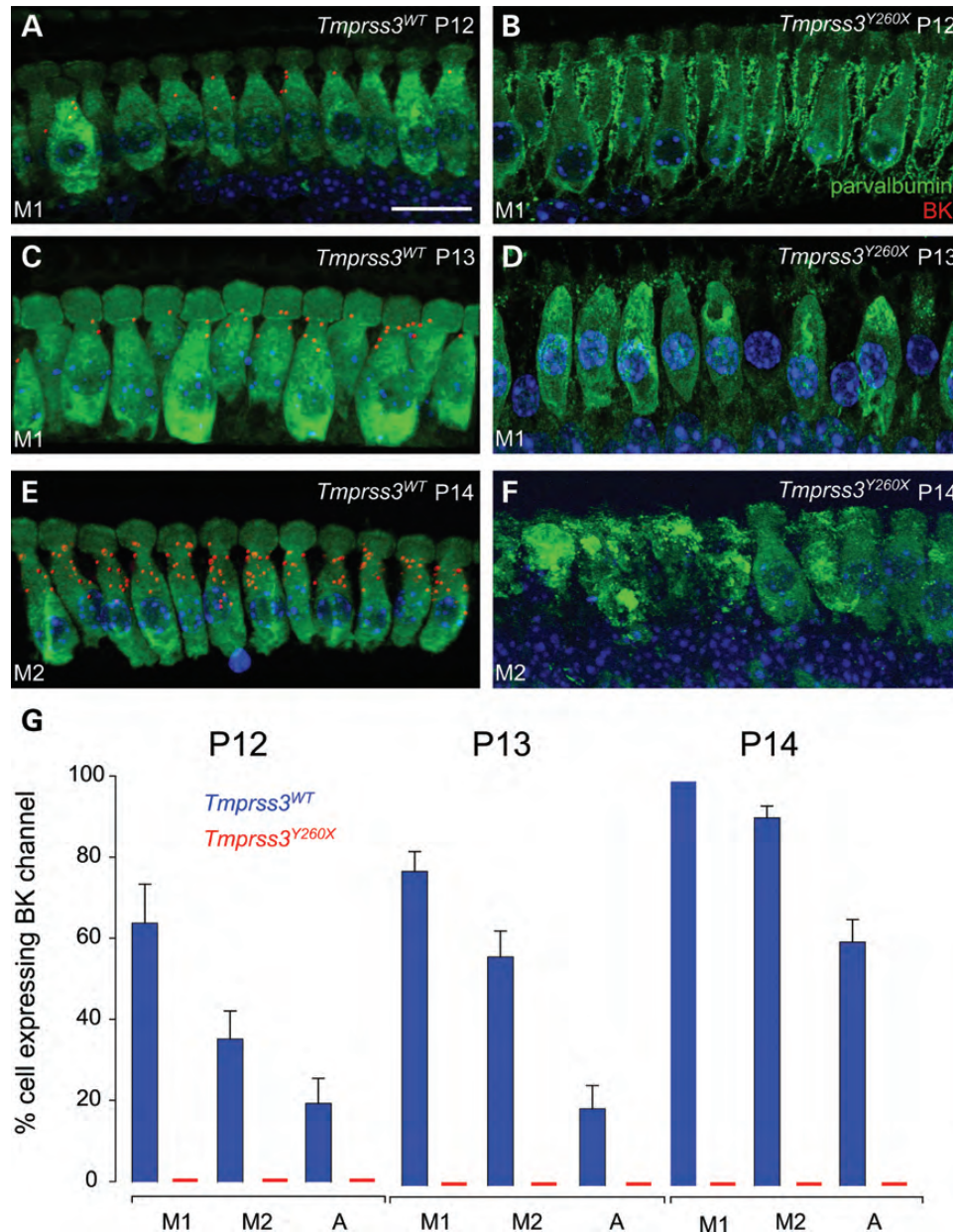


Figure 4. Kcnma1 channels are no longer expressed in the neck of IHCs of *Tmprss3*^{Y260X}-mutant mice. (A) Cochlear explants were stained with anti-Kcnma1 antibody (red) in P12 mice. IHCs were identified with parvalbumin staining using anti-parvalbumin monoclonal antibody (green), and the nucleus was stained with Hoechst. Kcnma1 channels were expressed in the neck of some IHCs from *Tmprss3*^{WT}. (B) In contrast, no Kcnma1 expression was found in the IHCs from P12 *Tmprss3*^{Y260X} mice. (C) Kcnma1 channels were more expressed in each P13 *Tmprss3*^{WT} IHC and in more IHCs of the same turn. (D) As for P12, no Kcnma1 labeling was found in *Tmprss3*^{Y260X} IHCs. (E) Kcnma1 channels were expressed in all P14 *Tmprss3*^{WT} IHCs of the same turn. (E) Like P13, no Kcnma1 labeling was found in *Tmprss3*^{Y260X} IHCs. (G) Quantification of Kcnma1 channel expression in the developing organ of Corti from P12 to 14 in three cochlear turns: M1, M2 and A (mid-turn 1, mid-turn 2 and apex). An increase in the number of IHCs expressing Kcnma1 channels was found from P12 to P14 in the *Tmprss3*^{WT} cochlea (blue vertical bar). The number of IHCs expressing channels was greater in the mid-turn than in the apex at the same developmental stage. In contrast, no Kcnma1 channel immunoreactivity was observed in any *Tmprss3*^{Y260X} IHCs (red line) ($n = 4$ for *Tmprss3*^{WT}, $n = 4$ for *Tmprss3*^{Y260X}). The difference is statistically significant (two sample *t*-test, $P < 0.05$).

Kcnma1 channels) as observed in *Tmprss3*^{Y260X} mice, but I_{Ca} current and exocytosis fail to mature in *Eps8* knockout mice in contrast to *Tmprss3*^{Y260X} mice. These data suggest that the same phenotype (lack of Kcnma1) is due to two different mechanisms. Finally, *SERPINB6*-truncating mutation is associated with DFN91 deafness (32). Serpinb6 is a proteinase inhibitor of cathepsin G and kallikreins. It has been shown

that Serpinb6 exhibits a prosurvival function in *Caenorhabditis elegans* (33). In developing and in adult cochlea, Serpinb6 is expressed in cochlear hair cells, suggesting a critical role of the protein in hair cell physiology (32). Nevertheless, Serpinb6 has not yet been identified as a partner of Kcnma1, and no information could be found showing a link between Serpinb6 and surface membrane expression of Kcnma1.

The analysis of the proteomic approach underlies 14.3.3 β and 14.3.3 ζ as potential proteins functionally related to the *Tmprss3*^{Y260X} mutation. Considering the IHC *Kcnma1* channel plasma membrane alteration, it is tempting to speculate that 14.3.3 proteins may be involved. Indeed, it has been shown that 14.3.3 β , 14.3.3 ϵ , 14.3.3 η , 14.3.3 γ , 14.3.3 τ and 14.3.3 ζ interact with *Kcnma1* channels and that downregulation of 14.3.3 γ induces an increase in *Kcnma1* channel membrane expression in CHO cells (27). 14.3.3 β knockdown increases ENaC membrane expression (34), 14.3.3 β mediates forward trafficking to the plasma membrane of KCNK3 (35) and 14.3.3 ζ mediates trafficking to the plasma membrane of KA2 kainate receptors (36). Moreover, 14-3-3 proteins promote the cell surface transport of correctly assembled complexes (37). Interestingly, cleavage of 14-3-3 proteins, which is executed by at least two different mechanisms, probably involves caspase-3 and a still unknown protease beyond the caspase family in an isoform-specific manner (38) that could be *Tmprss3*. Of course, we cannot rule out the possibility that *Tmprss3* directly controls the membrane expression level of *Kcnma1* channels, as *Tmprss3* and *Kcnma1* channels co-localize in the ER of transfected cells.

This novel link between *Kcnma1* channels and a type II serine protease may be highly significant in other organs, as *Kcnma1* channels are widely expressed in neuronal and non-neuronal tissues, including epithelia, smooth muscle cells and sensory cells, where they couple membrane potential and intracellular Ca²⁺ concentration (39–41). *Kcnma1* channels contribute to the repolarization of action potentials (APs) (42), mediate the fast phase after hyperpolarization following an AP (43–45), shape the dendritic Ca²⁺ spikes (46) and influence the release of neurotransmitters (47). Achieving a better understanding of the role of *Kcnma1* channels is important not only for furthering our knowledge of the involvement of these channels in physiologic processes but also for pathophysiologic conditions that have been demonstrated by recent discoveries implicating these channels in neurologic disorders. Indeed, autism and mental retardation have been linked to haploinsufficiency of the *Slo1* gene and decreased *Kcnma1* channel expression (48). In addition, *Kcnma1* channel mutations have been identified through genetic screening of a family with generalized epilepsy and paroxysmal dyskinesia (14).

In conclusion, our experiments indicate that *Tmprss3* deficiency causes a selective lack of functional *Kcnma1* channels. Future experiments will be required to clarify the exact mechanism by which *Tmprss3* regulates the abundance of functional *Kcnma1* channels in IHCs. However, the data presented here already strongly suggests that *Tmprss3* must be considered as an important factor for the proper functioning of hair cells.

MATERIALS AND METHODS

Animal handling

The care and use of animals followed the animal welfare guidelines of the 'Institut National de la Santé et de la Recherche Medicale' (Inserm), under the approval of the French 'Ministère

de l'Alimentation, de l'Agriculture et de la Pêche.' All efforts were made to minimize the number of animals used and their suffering. *Tmprss3*^{Y260X} mice were described previously by Fasquelle *et al.* (9).

Preparation of mouse inner ear extracts for proteomics analysis

Cochleae were isolated from 15 10-day-old mice of each genotype (WT and mutant) in cold PBS, and the bone was removed. The dissected cochleae were rinsed in water and wiped with paper before being placed in a microcentrifuge tube and weighed. The cochleae pellets were then frozen in liquid nitrogen and stored at -80°C . According to their weight, the pellets were resuspended in a defined volume of buffer (100 μl /10 mg of tissue) containing 8 M urea, 2 M thio-urea, 4% w/v CHAPS, 65 mM dithioerythritol (DTE), 40 mM Tris and protease inhibitors (Roche Diagnostics, Meylan, France) and sonicated for 3×10 s pulses at 20 kHz (Vibracell 72446, Fisher Scientific, Illkirch, France). After solubilization at room temperature (RT) on a rotating wheel for 2 h, the samples were centrifuged at 20 000g for 30 min, and the supernatants were collected and stored at -80°C until use. The amount of protein was estimated using a modified Bradford method (49).

2D-GE of proteins

Precast IPG strips (18 cm) with a non-linear immobilized pH 3–10 gradient were rehydrated with 70 μg of protein sample in 8 M urea, 2 M thiourea, 4% w/v CHAPS, 65 mM DTE, 0.0025% v/v bromophenol blue, and 1% v/v IPG buffer (3–10) overnight (50). Isoelectric focusing (IEF) was carried out on the EttanTM IPGphorTM IEF system at 20°C using a gradient mode to a total amount of 50 kVh. After the first dimensional run, the proteins were reduced (65 mM DTT in 6 M urea, 50 mM Tris–HCl, pH 8.8, 30% v/v glycerol, 2% w/v SDS and 0.001 v/v bromophenol blue) and then alkylated for 10 min in a similar buffer containing 135 mM iodoacetamide instead of DTT. Subsequently, the proteins were separated in the second dimension on homemade 12% SDS-polyacrylamide gels using an ISO-DALT electrophoresis unit at a constant voltage of 120 V at 10°C overnight. Analytical gels were stained with a Sypro Ruby fluorescence dye (Bio-Rad, Hercules, CA, USA) according to the manufacturer's instructions. At least five biologic replicates per genotype (*Tmprss3*^{WT} and *Tmprss3*^{Y260X}) were performed simultaneously to guarantee reproducible results. Each biologic sample was composed of a pool of six individual cochleae corresponding to three animals.

Image analysis

Gels were digitalized individually with a Typhoon 9400 laser scanner (GE Healthcare Life Sciences, Piscataway, NJ, USA) at 50 μm resolution with a photo multiplier tube voltage adjusted for maximum range without signal saturation. Images were stored as 16-bit gel files and then analyzed using the Progenesis Samespot[®] software v3.0 (Nonlinear Dynamics, Durham, UK). Images were warped for accurate alignment and spots were then detected automatically. Progenesis

Samespot[®] is based on the concept of recursive gel matching, which means that each gel in a matching set is used recursively as 'reference gel' once during the matching process. The quality of the automatic match was evaluated critically in each case, and if necessary, corrections were made manually.

Statistics

All statistics and figures were computed using the 'R/Bioconductor' statistical open source software (51) and the JMP v8 software (SAS Institute, Inc.). The differential intensity levels of protein spots between the *Tmprss3^{WT}* and *Tmprss3^{Y260X}* samples were analyzed by the non-parametric Wilcoxon rank sum test (also called the Mann–Whitney *U*-test). A *P*-value less than 0.05 was considered statistically significant. The area under the curve (AUC) receiver operating characteristic (ROC) was also calculated with the ROC package, and an AUC ROC value greater than 0.800 was considered significant.

Hierarchical ascendant clustering (HAC) analysis

Hierarchical ascendant clustering (HAC) is a method of cluster analysis based on a pairwise distance matrix, which builds a hierarchy of clusters with sequentially agglomerative and divisive approaches. We used this method to organize the map and to group the spots according to the nearest level of intensity. For this analysis, raw data were mean centered, and the Pearson correlation matrix and average linkage were chosen as parameters.

Protein identification

Spots of interest were excized from preparative gels with a ProPic robot (Perkin-Elmer, Wellesley, MA, USA). All subsequent steps were done automatically using a Multiprobe II robot (Perkin-Elmer). Spots were first washed with 300 μ l of water and then 300 μ l of 25 mM NH₄HCO₃. Destaining was performed twice in the presence of 300 μ l of 50% acetonitrile in 25 mM NH₄HCO₃. Gel pieces were then dehydrated twice using 300 μ l of 100% CH₃CN and finally dried at 37°C for 1 h. Eight microliters of a trypsin solution (Sequencing grade modified trypsin, Promega, Madison, USA) at a concentration of 0.0125 μ g/ μ l in 25 mM NH₄HCO₃ was added to every spot. Digestion was performed overnight at 37°C and stopped by the addition of 2 μ l of 2% formic acid. Digests were sonicated in an ultrasonic bath for 10 min, and supernatants were transferred into HPLC polypropylene tubes.

Protein digests were analyzed using a high-capacity ion trap mass spectrometer (Esquire HCT; Bruker Daltonik GmbH, Bremen, Germany) and interfaced with a nano-HPLC Chip-Cube system (Agilent Technologies, Santa Clara, USA). The chips contained both the pre-column and the column (Zorbax 300SB-C18; Agilent Technologies). Samples were first loaded onto the 4 mm enrichment cartridge at a flow rate of 4 μ l/min using 0.1% formic acid. After pre-concentration, peptides were separated on the column (75 μ m diameter and 43 mm length) at a flow rate of 0.3 μ l/min using a 15 min linear gradient from 3 to 80% acetonitrile in 0.1% formic acid and eluted into the mass spectrometer. A capillary voltage of 1.8–2.1 kV in the positive ion mode was used

together with a dry gas flow rate of 4.5 l/min at 250°C. A first full-scan mass spectrum was measured in the 310–1800 *m/z* range, followed by a second scan at higher resolution to measure precisely the mass of the three major ions in the previous scan. Finally, a third scan was performed to acquire the collision-induced MS/MS spectra of the selected ions. MS/MS raw data were analyzed using the data analysis software (Bruker Daltonik GmbH, Bremen, Germany) to generate the peak lists. The NCBI non-redundant database (NCBI nr, release 20101018) was queried locally using the Mascot search engine (v. 2.2.04; Matrix Science, London, UK) with the following parameters: Mus for the taxonomy, trypsin as the enzyme, one missed cleavage allowed, carbamidomethylation of Cysteine as a fixed modification, oxidation of Methionine as a variable modification, and 0.6 Da mass accuracy in both MS and MS/MS. Under these conditions, individual ion scores above 38 indicated identity or extensive homology (*P* < 0.05), and proteins were validated once they showed at least 1 peptide over this threshold.

Protein interaction data and network visualization

The gene names of the identified proteins were used to perform GO enrichment analysis using the Ontologizer software. This Java Web Start application allows the statistical analysis of sets of proteins or genes of interest mapped onto GO terms (<http://compbio.charite.de/ontologizer>) (52). GO annotation files (gene_association.wb and gene_ontology_edit.obo) were downloaded from www.geneontology.org in October 2011. The ontologizer was run using the following parameters: biologic process, parent–child union and the Benjamin–Hochberg statistical test. Biologic processes showing *P*-values below 0.05 were considered statistically significant. The ontologizer allows visualization of data as a directed acyclic graph highlighting all significantly enriched GO terms, in turn linked to the genes/proteins of interest.

PPI data were combined with our set of identified proteins to build a functional network. Full PPI datasets were available from two different open source literature-curated protein interaction databases: IntAct (<http://www.ebi.ac.uk/intact/site/index.jsf>; dated March 28 2011) and the Biological General Repository for Interaction Datasets (BioGRID; <http://thebiogrid.org/>; version 3.1.74). PPI networks were generated using Cytoscape (53), an open source software (<http://www.cytoscape.org/>; version 2.8.1). The gene names of all identified proteins were imported into IntAct via its Cytoscape plug-in. BioGRID datasets from *Mus musculus* (file BIOGRID-ORGANISM-Mus_musculus-3.1.74.tab) were imported into Cytoscape via the BioGRID plug-in (BioGridPlugin2). Proteins were represented by nodes and the interactions by edges. Then, for each of identified proteins, the direct interacting neighbors were identified (length = 1). Finally, the PPI networks from the IntAct and BioGRID databases were merged with an advanced merge network plug-in and displayed with Cytoscape using the edge-unweighted spring embedded style. The selection of subnetworks was based on the degree of connectivity of a significant number of identified proteins. Highly connected proteins were named 'hubs proteins.'

Immunohistochemistry and confocal imaging

Cochleae were extracted from the temporal bones of 12-, 13- or 14-day-old mice and fixed in cold 4% paraformaldehyde for 1 h with shaking. After several washes in PBS, organs of Corti were isolated from the stria vascularis and modiolus and incubated in a goat serum dilution buffer (GSDB) (16% normal goat serum, 450 mM NaCl, 0.3% Triton X-100, and 20 mM phosphate buffer, pH 7.4) at RT for 1 h. Anti-Kcnma1 rabbit antibody (Sigma Aldrich, St. Louis, MO, USA), anti-APOA1 goat antibody (Novus Biologicals, Cambridge, UK) that was successfully used in mouse (54,55) and anti-parvalbumin mouse antibody (Swant, Marly, Switzerland) were diluted in GSDB at 1/2000, 1/500 and 1/750, respectively and applied overnight at 4°C with shaking. After washing with washing buffer (450 mM NaCl, 20 mM phosphate buffer pH 7.4 and 0.3% Triton X-100) (6x 10 min with shaking), the organs of Corti were incubated with goat anti-rabbit and goat anti-mouse antibodies, respectively, coupled with Alexa Fluor-594 and -488 (Jackson ImmunoResearch Laboratories, Suffolk, UK) diluted at 1/3000 in GSDB for 1 h 30 at RT with shaking and protection from light. A 5 min supplementary incubation was carried out after the addition of Hoechst (FluoProbes, Interchim, Montluçon, France) at 1/200. After three 10 min washes each in a washing buffer, the organs of Corti were washed for 10 min in 5 mM phosphate buffer, pH 7.4, placed onto a glass microscope slide in a DaKo fluorescent mounting medium (DakoCytomation, Trappes, France) and covered with a thin glass coverslip. Confocal images were acquired using a laser scanning confocal microscope LSM 510 (Zeiss, LE PECQ, France) with argon and helium–neon lasers for excitation. Oil immersion objectives with a magnification of 63× were used, and Z-stacks were acquired using a step size of 1.5 μm. Three-dimensional reconstruction images were made using the Imaris software. No immunoreactivity was detected in the absence of the primary antibodies.

The intensity of APOA1 immunolabeling was quantified from red green blue confocal images using custom-made program written in MATLAB (The Mathworks). The APOA1-labeled voxels (red channel) localized in IHC cytoplasm (green channel) were (i) isolated using parvalbumin immunolabeling as a mask and (ii) used to calculate the mean intensity. Mean intensities were calculated in *Tmprss3^{WT}* ($n = 3$) and *Tmprss3^{Y260X}* animals ($n = 4$) and compared with Mann–Whitney–Wilcoxon test. These numbers correspond to the number of measurements. Each measurement contains at least five hair cells.

As mouse cochlea length has been found to average 6 mm (56), including the basal (3 mm), the middle (2 mm) and the apical (1 mm) coils, and as the IHCs have already degenerated at P12, the counting of the number of IHCs expressing Kcnma1 channels was achieved in middle turn (separated into two, M1 and M2) and in the apical turn (A).

Patch-clamp recordings

After cervical dislocation of the *Tmprss3^{WT}* and *Tmprss3^{Y260X}* mice (postnatal day 13, P13), IHCs of the apical coil of freshly dissected organs of Corti were patch clamped at RT in whole-cell configuration. The pipette solution contained (in mM) 135

KCl, 10 Hepes buffer, 1 MgCl₂, 2 Mg-ATP, 0.3 Na-GTP and 5 ethyleneglycol-bis(β-aminoethyl ether)-N,N,N',N'-tetraacetic acid. The extracellular solution contained (in mM) 144 NaCl, 5.8 KCl, 0.9 MgCl₂, 10 HEPES, 1.3 CaCl₂ and 10 D-glucose. The solutions were adjusted to pH 7.2 with osmolarities between 290 and 310 mOsmol/l. All chemicals were obtained from Sigma (Sigma Aldrich). The EPC-10 amplifier (HEKA, Lambrecht, Germany), controlled by the Patchmaster software (HEKA), was used for recording measurements. For K⁺ currents, series resistance (R_s) compensation was applied to 60%. The voltage was corrected offline for the voltage drop across uncompensated series resistance. Currents were low-pass filtered at 5 kHz and sampled at 50 kHz. All voltages were corrected for liquid junction potentials calculated between the pipette and the bath (4 mV). Currents were leak corrected using a p/10 protocol (usually 10 leak pulses with amplitudes of 20% of the original pulse from a holding potential of -104 mV). Cells that displayed a membrane current exceeding -50 pA at -74 mV were discarded from the analysis.

AUTHORS' CONTRIBUTIONS

B.D. designed research; L.M., L.F., R.N. and N.S. performed research; L.M., L.F., R.N. and N.S. analyzed the data; M.G. and H.S.S. contributed new reagents; and L.M., R.N., F.M., M.G., H.S.S., J.L.P. and B.D. wrote this paper.

SUPPLEMENTARY MATERIAL

Supplementary Material is available at *HMG* online.

ACKNOWLEDGEMENTS

We thank the Cellular Imaging Facility especially Chamroeu Sar and the Animal Facility of the INM. We thank Jérôme Bourien for the immunohistochemistry quantification of APOA1 and Frédéric Marmigère, Cédric Raoul and Alain Garcès for their critical review of the manuscript and for helpful discussions. The MS and MS/MS analyses were performed in the Proteomics Pole of Montpellier supported by the Région Languedoc-Roussillon and IBISA.

Conflict of Interest statement. None declared.

FUNDING

This work was supported by grants from the Swiss National Science Foundation (3100A0-114077-1 to M.G.); the National Health and Medical Research Council of Australia (257501, 215305, 71601 and 461204 to H.S.S.); and the Région Languedoc-Roussillon (Chercheur d'Avenir to B.D.).

REFERENCES

- Housley, G.D., Marcotti, W., Navaratnam, D. and Yamoah, E.N. (2006) Hair cells—beyond the transducer. *J. Membr. Biol.*, **209**, 89–118.
- Kros, C.J. (2007) How to build an inner hair cell: challenges for regeneration. *Hear. Res.*, **227**, 3–10.

3. Kros, C.J., Ruppersberg, J.P. and Rusch, A. (1998) Expression of a potassium current in inner hair cells during development of hearing in mice. *Nature*, **394**, 281–284.
4. Oliver, D., Taberner, A.M., Thurm, H., Sausbier, M., Arntz, C., Ruth, P., Fakler, B. and Liberman, M.C. (2006) The role of BKCa channels in electrical signal encoding in the mammalian auditory periphery. *J. Neurosci.*, **26**, 6181–6189.
5. Marcotti, W., Johnson, S.L., Holley, M.C. and Kros, C.J. (2003) Developmental changes in the expression of potassium currents of embryonic, neonatal and mature mouse inner hair cells. *The J. Physiol.*, **548**, 383–400.
6. Oliver, D., Knipper, M., Derst, C. and Fakler, B. (2003) Resting potential and submembrane calcium concentration of inner hair cells in the isolated mouse cochlea are set by KCNQ-type potassium channels. *J. Neurosci.*, **23**, 2141–2149.
7. Kubisch, C., Schroeder, B.C., Friedrich, T., Lutjohann, B., El-Amraoui, A., Marlin, S., Petit, C. and Jentsch, T.J. (1999) KCNQ4, a novel potassium channel expressed in sensory outer hair cells, is mutated in dominant deafness. *Cell*, **96**, 437–446.
8. Scott, H.S., Kudoh, J., Wattenhofer, M., Shibuya, K., Berry, A., Chrast, R., Guipponi, M., Wang, J., Kawasaki, K., Asakawa, S. *et al.* (2001) Insertion of beta-satellite repeats identifies a transmembrane protease causing both congenital and childhood onset autosomal recessive deafness. *Nat. Genet.*, **27**, 59–63.
9. Fasquelle, L., Scott, H.S., Lenoir, M., Wang, J., Rebillard, G., Gaboyard, S., Venteo, S., Francois, F., Mausset-Bonfont, A.L., Antonarakis, S.E. *et al.* (2011) Tmprss3, a transmembrane serine protease deficient in human DFNB8/10 deafness, is critical for cochlear hair cell survival at the onset of hearing. *J. Biol. Chem.*, **286**, 17383–17397.
10. Guipponi, M., Vuagniaux, G., Wattenhofer, M., Shibuya, K., Vazquez, M., Dougherty, L., Scamuffa, N., Guida, E., Okui, M., Rossier, C. *et al.* (2002) The transmembrane serine protease (TMPRSS3) mutated in deafness DFNB8/10 activates the epithelial sodium channel (ENaC) in vitro. *Hum. Mol. Genet.*, **11**, 2829–2836.
11. Sokolowski, B., Duncan, R.K., Chen, S., Karolat, J., Kathiresan, T. and Harvey, M. (2009) The large-conductance Ca(2+)-activated K(+) channel interacts with the apolipoprotein ApoA1. *Biochem. Biophys. Res. Commun.*, **387**, 671–675.
12. Robitaille, R., Garcia, M.L., Kaczorowski, G.J. and Charlton, M.P. (1993) Functional colocalization of calcium and calcium-gated potassium channels in control of transmitter release. *Neuron*, **11**, 645–655.
13. Brayden, J.E. and Nelson, M.T. (1992) Regulation of arterial tone by activation of calcium-dependent potassium channels. *Science*, **256**, 532–535.
14. Burdiga, T. and Wray, S. (2005) Action potential refractory period in ureter smooth muscle is set by Ca sparks and BK channels. *Nature*, **436**, 559–562.
15. Ahluwalia, J., Tinker, A., Clapp, L.H., Duchon, M.R., Abramov, A.Y., Pope, S., Nobles, M. and Segal, A.W. (2004) The large-conductance Ca2+-activated K+ channel is essential for innate immunity. *Nature*, **427**, 853–858.
16. Couloigner, V., Fay, M., Djelidi, S., Farman, N., Escoubet, B., Runembert, I., Sterkers, O., Friedlander, G. and Ferrary, E. (2001) Location and function of the epithelial Na channel in the cochlea. *Am. J. Physiol.*, **280**, F214–F222.
17. Grunder, S., Muller, A. and Ruppersberg, J.P. (2001) Developmental and cellular expression pattern of epithelial sodium channel alpha, beta and gamma subunits in the inner ear of the rat. *The Eur. J. Neurosci.*, **13**, 641–648.
18. Zhong, S.X. and Liu, Z.H. (2004) Immunohistochemical localization of the epithelial sodium channel in the rat inner ear. *Hear. Res.*, **193**, 1–8.
19. Pyott, S.J., Glowatzki, E., Trimmer, J.S. and Aldrich, R.W. (2004) Extrasynaptic localization of inactivating calcium-activated potassium channels in mouse inner hair cells. *J. Neurosci.*, **24**, 9469–9474.
20. Brandt, A., Striessnig, J. and Moser, T. (2003) CaV1.3 channels are essential for development and presynaptic activity of cochlear inner hair cells. *J. Neurosci.*, **23**, 10832–10840.
21. Marcotti, W., Erven, A., Johnson, S.L., Steel, K.P. and Kros, C.J. (2006) Tmc1 is necessary for normal functional maturation and survival of inner and outer hair cells in the mouse cochlea. *J. Physiol.*, **574**, 677–698.
22. Neef, J., Gehrt, A., Bulankina, A.V., Meyer, A.C., Riedel, D., Gregg, R.G., Strenzke, N. and Moser, T. (2009) The Ca2+ channel subunit beta2 regulates Ca2+ channel abundance and function in inner hair cells and is required for hearing. *J. Neurosci.*, **29**, 10730–10740.
23. Roux, I., Hosie, S., Johnson, S.L., Bahloul, A., Cayet, N., Nouaille, S., Kros, C.J., Petit, C. and Safieddine, S. (2009) Myosin VI is required for the proper maturation and function of inner hair cell ribbon synapses. *Hum. Mol. Genet.*, **18**, 4615–4628.
24. Zampini, V., Ruttiger, L., Johnson, S.L., Franz, C., Furness, D.N., Waldhaus, J., Xiong, H., Hackney, C.M., Holley, M.C., Offenhauser, N. *et al.* (2011) Eps8 regulates hair bundle length and functional maturation of mammalian auditory hair cells. *PLoS Biol.*, **9**, e1001048.
25. Rusch, A., Ng, L., Goodyear, R., Oliver, D., Lisoukov, I., Vennstrom, B., Richardson, G., Kelley, M.W. and Forrest, D. (2001) Retardation of cochlear maturation and impaired hair cell function caused by deletion of all known thyroid hormone receptors. *J. Neurosci.*, **21**, 9792–9800.
26. Kathiresan, T., Harvey, M., Orchard, S., Sakai, Y. and Sokolowski, B. (2009) A protein interaction network for the large conductance Ca(2+)-activated K(+) channel in the mouse cochlea. *Mol. Cell. Proteomics*, **8**, 1972–1987.
27. Sokolowski, B., Orchard, S., Harvey, M., Sridhar, S. and Sakai, Y. (2011) Conserved BK channel-protein interactions reveal signals relevant to cell death and survival. *PLoS One*, **6**, e28532.
28. Zhu, M., Yang, T., Wei, S., DeWan, A.T., Morell, R.J., Efenbein, J.L., Fisher, R.A., Leal, S.M., Smith, R.J. and Friderici, K.H. (2003) Mutations in the gamma-actin gene (ACTG1) are associated with dominant progressive deafness (DFNA20/26). *Am. J. Hum. Genet.*, **73**, 1082–1091.
29. Riviere, J.B., van Bon, B.W., Hoischen, A., Kholmanskikh, S.S., O’Roak, B.J., Gilissen, C., Gijsen, S., Sullivan, C.T., Christian, S.L., Abdul-Rahman, O.A. *et al.* (2012) De novo mutations in the actin genes ACTB and ACTG1 cause Baraitser-Winter syndrome. *Nat. Genet.*, **44**, 440–444, S441–442.
30. Perrin, B.J., Sonnemann, K.J. and Ervasti, J.M. (2010) beta-actin and gamma-actin are each dispensable for auditory hair cell development but required for Stereocilia maintenance. *PLoS Genet.*, **6**, e1001158.
31. Kim, E.Y., Suh, J.M., Chiu, Y.H. and Dryer, S.E. (2010) Regulation of podocyte BK(Ca) channels by synaptopodin, Rho, and actin microfilaments. *Am. J. Physiol.*, **299**, F594–F604.
32. Sirmaci, A., Erbek, S., Price, J., Huang, M., Duman, D., Cengiz, F.B., Bademci, G., Tokgoz-Yilmaz, S., Hismi, B., Ozdag, H. *et al.* (2010) A truncating mutation in SERPINB6 is associated with autosomal-recessive nonsyndromic sensorineural hearing loss. *Am. J. Hum. Genet.*, **86**, 797–804.
33. Luke, C.J., Pak, S.C., Askew, Y.S., Naviglia, T.L., Askew, D.J., Nobar, S.M., Vetica, A.C., Long, O.S., Watkins, S.C., Stolz, D.B. *et al.* (2007) An intracellular serpin regulates necrosis by inhibiting the induction and sequelae of lysosomal injury. *Cell*, **130**, 1108–1119.
34. Liang, X., Butterworth, M.B., Peters, K.W., Walker, W.H. and Frizzell, R.A. (2008) An obligatory heterodimer of 14-3-3beta and 14-3-3epsilon is required for aldosterone regulation of the epithelial sodium channel. *J. Biol. Chem.*, **283**, 27418–27425.
35. O’Kelly, I., Butler, M.H., Zilberberg, N. and Goldstein, S.A. (2002) Forward transport. 14-3-3 binding overcomes retention in endoplasmic reticulum by dibasic signals. *Cell*, **111**, 577–588.
36. Vivithanaporn, P., Yan, S. and Swanson, G.T. (2006) Intracellular trafficking of KA2 kainate receptors mediated by interactions with coatomer protein complex I (COPI) and 14-3-3 chaperone systems. *J. Biol. Chem.*, **281**, 15475–15484.
37. Heusser, K., Yuan, H., Neagoe, I., Tarasov, A.I., Ashcroft, F.M. and Schwappach, B. (2006) Scavenging of 14-3-3 proteins reveals their involvement in the cell-surface transport of ATP-sensitive K+ channels. *J. Cell Sci.*, **119**, 4353–4363.
38. Kuzelova, K., Grebenova, D., Pluskalova, M., Kavan, D., Halada, P. and Hrkal, Z. (2009) Isoform-specific cleavage of 14-3-3 proteins in apoptotic JURL-MK1 cells. *J. Cell. Biochem.*, **106**, 673–681.
39. Fettiplace, R. and Fuchs, P.A. (1999) Mechanisms of hair cell tuning. *Ann. Rev. Physiol.*, **61**, 809–834.
40. Petersen, O.H. and Maruyama, Y. (1984) Calcium-activated potassium channels and their role in secretion. *Nature*, **307**, 693–696.
41. Vergara, C., Latorre, R., Marrion, N.V. and Adelman, J.P. (1998) Calcium-activated potassium channels. *Curr. Opin. Neurobiol.*, **8**, 321–329.
42. Storm, J.F. (1987) Action potential repolarization and a fast after-hyperpolarization in rat hippocampal pyramidal cells. *J. Physiol.*, **385**, 733–759.

43. Coling, D.E., Ding, D., Young, R., Lis, M., Stofko, E., Blumenthal, K.M. and Salvi, R.J. (2007) Proteomic analysis of cisplatin-induced cochlear damage: methods and early changes in protein expression. *Hear. Res.*, **226**, 140–156.
44. Lancaster, B. and Nicoll, R.A. (1987) Properties of two calcium-activated hyperpolarizations in rat hippocampal neurones. *J. Physiol.*, **389**, 187–203.
45. Womack, M.D. and Khodakhah, K. (2002) Characterization of large conductance Ca²⁺-activated K⁺ channels in cerebellar Purkinje neurons. *Eur. J. Neurosci.*, **16**, 1214–1222.
46. Golding, N.L., Jung, H.Y., Mickus, T. and Spruston, N. (1999) Dendritic calcium spike initiation and repolarization are controlled by distinct potassium channel subtypes in CA1 pyramidal neurons. *J. Neurosci.*, **19**, 8789–8798.
47. Yazejian, B., Sun, X.P. and Grinnell, A.D. (2000) Tracking presynaptic Ca²⁺ dynamics during neurotransmitter release with Ca²⁺-activated K⁺ channels. *Nat. Neurosci.*, **3**, 566–571.
48. Laumonier, F., Roger, S., Guerin, P., Molinari, F., M'Rad, R., Cahard, D., Belhadj, A., Halayem, M., Persico, A.M., Elia, M. *et al.* (2006) Association of a functional deficit of the BKCa channel, a synaptic regulator of neuronal excitability, with autism and mental retardation. *Am. J. Psychiatry*, **163**, 1622–1629.
49. Weekes, J., Wheeler, C.H., Yan, J.X., Weil, J., Eschenhagen, T., Scholtysik, G. and Dunn, M.J. (1999) Bovine dilated cardiomyopathy: proteomic analysis of an animal model of human dilated cardiomyopathy. *Electrophoresis*, **20**, 898–906.
50. Molina, L., Grimaldi, M., Robert-Hebmann, V., Espert, L., Varbanov, M., Devaux, C., Granier, C. and Biard-Piechaczyk, M. (2007) Proteomic analysis of the cellular responses induced in uninfected immune cells by cell-expressed X4 HIV-1 envelope. *Proteomics*, **7**, 3116–3130.
51. Gentleman, R.C., Carey, V.J., Bates, D.M., Bolstad, B., Dettling, M., Dudoit, S., Ellis, B., Gautier, L., Ge, Y., Gentry, J. *et al.* (2004) Bioconductor: open software development for computational biology and bioinformatics. *Genome Biol.*, **5**, R80.
52. Bauer, S., Grossmann, S., Vingron, M. and Robinson, P.N. (2008) Ontologizer 2.0—a multifunctional tool for GO term enrichment analysis and data exploration. *Bioinformatics*, **24**, 1650–1651.
53. Cline, M.S., Smoot, M., Cerami, E., Kuchinsky, A., Landys, N., Workman, C., Christmas, R., Avila-Campilo, I., Creech, M., Gross, B. *et al.* (2007) Integration of biological networks and gene expression data using Cytoscape. *Nat. Protoc.*, **2**, 2366–2382.
54. Duong, P.T., Collins, H.L., Nickel, M., Lund-Katz, S., Rothblat, G.H. and Phillips, M.C. (2006) Characterization of nascent HDL particles and microparticles formed by ABCA1-mediated efflux of cellular lipids to apoA-I. *J. Lipid Res.*, **47**, 832–843.
55. Hasebe, A., Pennock, N.D., Mu, H.H., Chan, F.V., Taylor, M.L. and Cole, B.C. (2006) A microbial TLR2 agonist imparts macrophage-activating ability to apolipoprotein A-I. *J. Immunol.*, **177**, 4826–4832.
56. Ou, H.C., Harding, G.W. and Bohne, B.A. (2000) An anatomically based frequency-place map for the mouse cochlea. *Hear. Res.*, **145**, 123–129.